

Complex Structure of Triangular Graphene: Electronic, Magnetic and Electromechanical Properties

Motohiko Ezawa

Department of Applied Physics, University of Tokyo, Hongo 7-3-1, 113-8656, Japan

We have investigated electronic and magnetic properties of graphene nanodisks (nanosize triangular graphene) as well as electromechanical properties of graphene nanojunctions. Nanodisks are nanomagnets made of graphene, which are robust against perturbation such as impurities and lattice defects, where the ferromagnetic order is assured by Lieb's theorem. We can generate a spin current by spin filter, and manipulate it by a spin valve, a spin switch and other spintronic devices made of graphene nanodisks. We have analyzed nanodisk arrays, which have multi-degenerate perfect flat bands and are ferromagnet. By connecting two triangular graphene corners, we propose a nanomechanical switch and a rotator, which can detect a tiny angle rotation by measuring currents between the two corners. By making use of the strain induced Peierls transition of zigzag nanoribbons, we also propose a nanomechanical stretch sensor, in which the conductance can be switch off by a nanometer scale stretching.

Keyword: graphene, nanoribbons, nanodisks, graphene-nanodisk array, quasiferromagnet, spintronics, nanomechanics, electromechanics

I. INTRODUCTION

Graphene, which is a one-layer thick honeycomb structure of carbon, is an amazing material¹. Electrons exhibit high mobility and travel micron distances without scattering at room temperature. It is a very thin and strong material, showing very high thermal conductivity. Graphene is now a main topic of nanoscience.

Much attention has been focused on graphene nanoribbons, which is a one-dimensional ribbon-like derivatives of graphene. They have various band structure depending on the edge and width. In particular, zigzag graphene nanoribbons show edge ferromagnetism due to almost flat low-energy band at the Fermi level. There are a profusion of papers on them, among which we cite some of early works²⁻⁴. Another basic element of graphene derivatives is a graphene nanodisk⁵. It is a nanometer-scale disk-like material which has a closed edge. It may be considered as a giant molecule made of aromatic compound. It is possible to manufacture them by etching a graphene sheet by Ni nanoparticles⁶. Among them, trigonal zigzag nanodisks have a novel electric property that there exist half-filled zero-energy states in the non-interacting regime, as was revealed first by the tight-binding model⁵ and then by first-principle calculations⁷⁻⁹. Various remarkable properties of nanodisks have been investigated extensively in a series of works^{5,10-12}. Nanodisk is also referred to as nanoisland⁷, nanoflake^{9,13,14}, nanofragment¹⁵ or graphene quantum dot^{16,17}.

Nanoribbons and nanodisks correspond to quantum wires and quantum dots, respectively. They are candidates of future carbon-based nanoelectronics and spintronics alternative to silicon devices. A nanoribbon-nanodisk complex can in principle be fabricated, embodying various functions, only by etching a graphene sheet. Furthermore, graphene is common material and ecological. In this paper, exploring electronic, magnetic and electromechanical properties of trigonal zigzag graphene nanodisks [see Fig.1], we propose some application of nanodisk-nanoribbon complex to nanoelectronics, spintronics and electromechanics devices

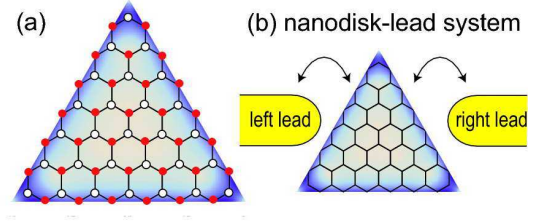


FIG. 1. (a) Geometric configuration of a trigonal zigzag nanodisk. The nanodisk size is defined by $N = N_{\text{ben}} - 1$ with N_{ben} the number of benzenes on one side of the trigon. Here, $N = 5$. The A (B) sites on the lattice are indicated by red dots (white circles). The electron density is found to be localized along the edges. (b) The nanodisk-lead system. A nanodisk is connected to the right and left leads by tunneling coupling. It may act as a spin filter.

II. ENERGY SPECTRUM

We calculate the energy spectrum of the nanodisk based on the nearest-neighbor tight-binding model, which has proved to describe accurately the electronic structure of graphene, carbon nanotubes, graphene nanoribbons and other sp^2 carbon materials. The Hamiltonian is defined by

$$H_0 = \sum_i \varepsilon_i c_i^\dagger c_i + \sum_{\langle i,j \rangle} t_{ij} c_i^\dagger c_j, \quad (1)$$

where ε_i is the site energy, t_{ij} is the transfer energy, and c_i^\dagger is the creation operator of the π electron at the site i . The summation is taken over all nearest neighboring sites $\langle i, j \rangle$. Owing to their homogeneous geometrical configuration, we may take constant values for these energies, $\varepsilon_i = \varepsilon_F$ and $t_{ij} = t \approx 2.70\text{eV}$. There exists one electron per one carbon, and the band-filling factor is $1/2$. Then, the diagonal term yields just a constant, $\varepsilon_F N_C$, and can be neglected in the Hamiltonian, where N_C is the number of carbon atoms.

We define the size N of a nanodisk by $N = N_{\text{ben}} - 1$, where N_{ben} is the number of benzenes on one side of the trigon as in Fig.1(a). It can be shown⁵ that the determinant associated with

the Hamiltonian (1) has such a factor as

$$\det[\varepsilon I - H(N_C)] \propto \varepsilon^N, \quad (2)$$

implying N -fold degeneracy of the zero-energy states. The gap energy is as large as a few eV for nanodisks with small N , where it is a good approximation to investigate the electron-electron interaction physics only in the zero-energy sector, by projecting the system to the subspace made of those zero-energy states. As we shall see in Section V, the approximation remains to be good even for those with large N .

III. TRIGONAL SYMMETRY

The symmetry group of a trigonal nanodisk is C_{3v} , which is generated by the $2\pi/3$ rotation c_3 and the mirror reflection σ_v . It has the representation $\{A_1, A_2, E\}$. The A_1 representation is invariant under the rotation c_3 and the mirror reflection σ_v . The A_2 representation is invariant under c_3 and antisymmetric under σ_v . The E representation acquires $\pm 2\pi/3$ phase shift under the $2\pi/3$ rotation. The A_1 and A_2 are 1-dimensional representations (singlets) and the E is a 2-dimensional representation (doublet). These properties are summarized in the following character table:

C_{3v}	ε	$2c_3$	$3\sigma_v$
A_1	1	1	1
A_2	1	1	-1
E	2	-1	0

(3)

The zero-energy sector consists of N orthonormal states. We are able to index them by the wave number k along the edge. It is a continuous parameter for an infinitely long graphene edge. According to the tight-binding-model result, the flat band emerges for

$$-\pi \leq ak < -2\pi/3 \quad \text{and} \quad 2\pi/3 < ak \leq \pi. \quad (4)$$

We focus on the wave function $\psi(x, y)$ at one of the A sites on an edge, and investigate the phase shift when we step over to the neighboring site [see Fig.1(a)]. There are N links along one edge of the size- N nanodisk, for which we obtain the phase shift Nak , where a is the spacing between the neighboring A sites and k is the wave number along the edge. On the other hand, the phase shift is π at the corner. The total phase shift is $3Nak + 3\pi$, when we encircle the nanodisk once. By requiring the single-valueness of the wave function, it is found to be quantized as

$$ak_n = \pm [(2n + 1)/3N + 2/3] \pi, \quad (5)$$

where it follows that $0 \leq n \leq (N - 1)/2$ from the allowed region (4) of the wave number.

We may group the states according to the trigonal symmetry (3). With respect to the rotation there are three elements c_3^0, c_3, c_3^2 , which correspond to $1, e^{2\pi i/3}, e^{4\pi i/3}$. Accordingly, the phase shift of one edge is $0, 2\pi/3, 4\pi/3$. The state is

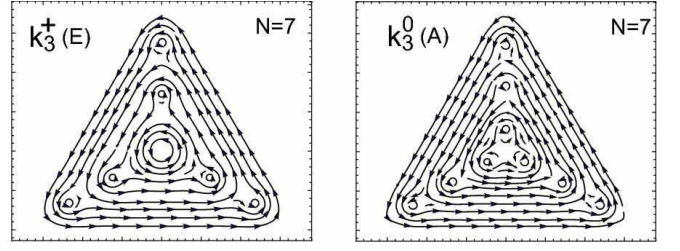


FIG. 2. Probability density flow for the zero-energy states in the nanodisk with $N = 7$. The representation of the trigonal symmetry group C_{3v} is indicated in the parenthesis. A vortex appears at the center of mass for the state belongs to the E (doublet) representation. The winding number at the center is 2 in the state $|k_n^\pm\rangle$.

grouped according to the representation of the trigonal symmetry group C_{3v} as follows,

$$\left. \begin{aligned} A_1 \text{ (singlet)} &: |k_n^0\rangle + |-k_n^0\rangle, \\ A_2 \text{ (singlet)} &: |k_n^0\rangle - |-k_n^0\rangle, \\ E \text{ (doublet)} &: |k_n^\pm\rangle, \quad |-k_n^\pm\rangle, \end{aligned} \right\} \text{ for } k_n^0 = \frac{6n + 3}{3Na} \pi, \\ \text{for } k_n^\pm = \frac{6n \pm 1}{3Na} \pi. \quad (6)$$

The zero-energy state is indexed by the quantized wave number as $|k_n^\alpha\rangle$ with (6).

To see the meaning of the wave number k_n^α more in detail¹², we have calculated the probability density flow,

$$\mathcal{A}_i(x, y) = -i\psi^*(x, y)\partial_i\psi(x, y) \quad (7)$$

for states $|k_n^\alpha\rangle$, which we show for the case of $N = 7$ in Fig.2. We observe clearly a texture of vortices. These vortices manifest themselves as magnetic vortices perpendicular to the nanodisk plane when the electromagnetic fields are coupled.

The total winding number N_{vortex} is calculated by

$$N_{\text{vortex}} = \frac{1}{2\pi} \oint dx_i \frac{\mathcal{A}_i(x, y)}{|\psi(x, y)|^2} = N + m - 1, \quad (8)$$

with $m = 0, 1, 2, \dots, \lfloor (N - 1)/2 \rfloor$ in the size- N nanodisk, where $\lfloor a \rfloor$ denotes the maximum integer equal to or smaller than a . We find $N_{\text{vortex}} = 3n$ for k_n^0 , $N_{\text{vortex}} = 3n + 1$ for k_{n+1}^- and $N_{\text{vortex}} = 3n + 2$ for k_n^+ . The wave functions are classified in terms of modulo of the total winding number: The wave function belongs to the E-representation and has chiral edge mode for $N_{\text{vortex}} \equiv 1, 2 \pmod{3}$, and belongs to the A-representation and has non-chiral edge mode for $N_{\text{vortex}} \equiv 0 \pmod{3}$. The winding number of the vortex at the center of the nanodisk is $0, 1, 2$ in the state $|k_n^0\rangle, |k_n^-\rangle, |k_n^+\rangle$, respectively.

IV. QUASIFERROMAGNET

The total spin of the ground state is determined by Lieb's theorem. The total spin is given by the difference of the A site and the B site, $S = \frac{1}{2}|N_A - N_B|$, where N_A and N_B are number of A site and B site. Here, $S = \frac{1}{2}N$ in the size- N nanodisk, where $N_A = (N + 1)(N + 6)/2$ and

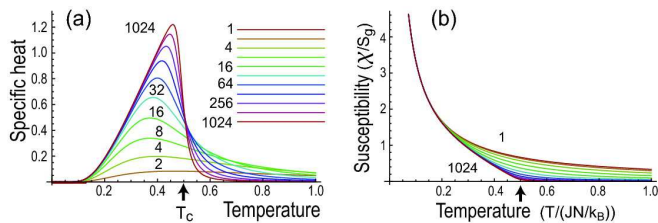


FIG. 3. Thermodynamical properties of the nanodisk-spin system. (a) The specific heat C in unit of $k_B N$. (b) The susceptibility χ in unit of S_g . The size is $N = 1, 2, 2^2, \dots, 2^{10}$. The horizontal axis stands for the temperature T in unit of JN/k_B . The arrow represents the phase transition point T_c in the limit $N \rightarrow \infty$.

$N_B = (N+2)(N+3)/2$. Hence we expect a nanodisk to act as a ferromagnet. The ferromagnetic ground state is robust against perturbations such as randomness and lattice defects since it is assured by Lieb's theorem. This feature brings out a remarkable contrast between nanodisks and nanoribbons. The ferromagnetic order is fragile due to the lack of Lieb's theorem in the case of nanoribbons.

We investigate ferromagnetic properties by introducing Coulomb interactions into the zero-energy sector⁵. We have calculated specific heats and susceptibilities at temperature T in Fig.3. There appear singularities in thermodynamical quantities as $N \rightarrow \infty$, which represent a phase transition at T_c between the ferromagnet and paramagnet states, where $T_c = JN/2k_B$. For finite N , there are steep changes around T_c , though they are not singularities. It is not a phase transition. However, it would be reasonable to call it a quasi-phase transition between the quasiferromagnet and paramagnet states. Such a quasi-phase transition is manifest even in finite systems with $N = 100 \sim 1000$.

The specific heat takes nonzero-value for $T > T_c$, as shown in Fig.3(a), which is zero in the limit $N \rightarrow \infty$. The result indicates the existence of some correlations in the paramagnet state. On the other hand, the susceptibility χ always shows the Curie-Weiss law $\chi \propto 1/T$ near $T = 0$, and exhibits also a behavior showing a quasi-phase transition at $T = T_c$, as shown in Fig.3(b). In the finite system, the expectation value of $S_{z,\text{tot}}$ is always zero because there is no spontaneous symmetry breakdown in the finite system, and the behavior is that of paramagnet.

V. MAGNETISM OF LARGE NANODISKS

For large N nanodisks, the band gap decreases inversely proportional to the size. One may wonder if our analysis based only on the zero-energy sector is valid. Indeed, the size of experimentally available nanodisks is as large as $N = 100 \sim 1000$. We wish to argue that our analysis based on the zero-energy sector is essentially correct, even if the size N of the nanodisk is large and the band gap becomes very narrow.

Near the Fermi energy, the density of states (DOS) $D(\varepsilon)$ consists of that of the bulk graphene and an additional peak at the zero-energy states due to the edge states for $N \gg 1$,

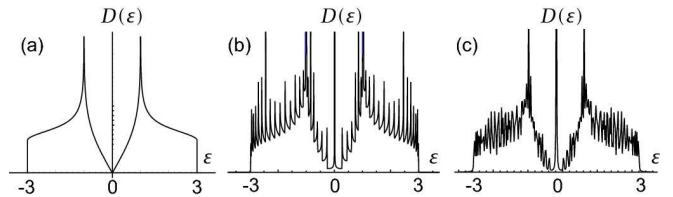


FIG. 4. The density of states of (a) graphene, (b) graphene nanoribbon and (c) graphene nanodisk. The horizontal axis is the energy ε in unit of t .

as illustrated in Fig.4. Hence, together with spin degrees of freedom, it behaves as

$$D(\varepsilon) = 2cN_C |\varepsilon| + 2N\delta(\varepsilon), \quad (9)$$

with a certain constant factor c . The linear term is due to the bulk states, and the Dirac delta function term is due to the edge states. The important point is that the edge-state peak is clearly distinguished from the DOS due to the bulk part. It is enough to take into account only the zero-energy sector to analyze physics near the Fermi energy, since the contribution from the edge states is dominant.

We calculate the magnetization of a nanodisk when its size is large. We start with the Hubbard Hamiltonian,

$$H = \sum_{k\sigma} \varepsilon(k) c_{k\sigma}^\dagger c_{k\sigma} + U \sum_{kk'q} c_{k+q\uparrow}^\dagger c_{k'-q\downarrow}^\dagger c_{k'\downarrow} c_{k\uparrow}. \quad (10)$$

Let $\langle n_\uparrow \rangle, \langle n_\downarrow \rangle$ be the average numbers of the up and down spins. The magnetization is given by $\langle m \rangle = \langle n_\uparrow \rangle - \langle n_\downarrow \rangle$. It is determined self-consistently by the relation

$$\langle m \rangle = \int d\varepsilon D(\varepsilon) [f(\varepsilon - \Delta) - f(\varepsilon + \Delta)], \quad (11)$$

in terms of the Fermi distribution function

$$f(x) = (\exp[(x - \mu)/k_B T] + 1)^{-1} \quad (12)$$

and

$$\Delta = \frac{U}{2N_C} \langle m \rangle + \frac{1}{2}h. \quad (13)$$

Substituting the formula (9) into the Stoner equation (11), we obtain

$$\langle m \rangle = N \tanh \frac{\beta\Delta}{2} + cN_C \left[\Delta^2 + \frac{1}{\beta^2} \left\{ \frac{\pi^2}{3} + 4\text{Li}_2(-e^{-\beta\Delta}) \right\} \right], \quad (14)$$

with the dilogarithm function $\text{Li}_2(x)$. It is difficult to solve this equation for $\langle m \rangle$ self-consistently at general temperature T . We examine two limits, $T \rightarrow 0$ and $T \rightarrow \infty$.

For the zero temperature ($T \rightarrow 0$) we obtain the magnetization as

$$\langle m \rangle = N + c \frac{U^2}{4N_C} \langle m \rangle^2 + \frac{cUh}{2} \langle m \rangle + O(h^2). \quad (15)$$

Because $|\langle m \rangle| \leq N$, it follows that $\langle m \rangle = N + O(1)$. The contribution from the bulk gives a negligible correction to the

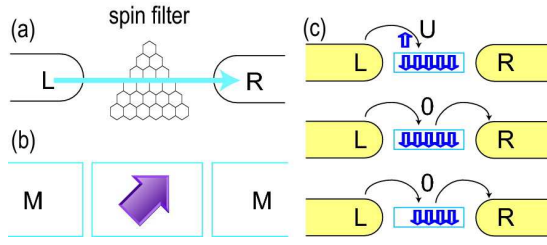


FIG. 5. (a) An electron tunnels from the left lead to the nanodisk and then to the right lead. The system is a reminiscence of a metal-ferromagnet-metal junction. (b) Only electrons with the same spin direction as the nanodisk spin can pass through the nanodisk freely. As a result, when we apply a spin-unpolarized current to the nanodisk, the outgoing current is spin polarized to the direction of the nanodisk spin. Consequently, this system acts as a spin filter.

total magnetization. Hence the magnetization is $\langle m \rangle = N$, and the ground state is fully polarized whenever $U \neq 0$. Ferromagnetism occurs irrespective of the strength of the Coulomb interaction. The magnetization is proportional not to N_C but N . In this sense the ground state of nanodisk is not bulk ferromagnet but surface ferromagnet, which is consistent with the previous result.

We next investigate the high temperature limit ($T \rightarrow \infty$). Using the Taylor expansion of the dilogarithm function,

$$\text{Li}_2(-e^{-\beta\Delta}) = -\frac{\pi^2}{12} + \beta\Delta \log 2 - \frac{\beta^2\Delta^2}{4} + \frac{\beta^3\Delta^3}{24} + \dots, \quad (16)$$

we find

$$\langle m \rangle = N \tanh \frac{\beta\Delta}{2} + cN_c \left[\frac{4\Delta}{\beta} \log 2 + \frac{\beta\Delta^3}{6} + \dots \right]. \quad (17)$$

The leading term is the second term, and hence the main contribution comes from the bulk. The solution is only $\langle m \rangle = 0$ for which $\Delta = 0$. There is no magnetization at high temperature.

A comment is in order. We have assumed that the magnetization axis is fixed and only longitudinal fluctuations of the magnetic moments take place. In general, spin-wave-like fluctuations are dominant at the edges of graphene¹⁸, because they are gapless Goldstone modes. On the contrary, there exist no gapless Goldstone modes in graphene nanodisks, because the edge is finite and closed. Furthermore, when the length of the edge is very small, spin-wave-like fluctuations have a large gap. Hence, our approximation is valid for nanodisks.

VI. APPLICATION FOR SPINTRONIC DEVICES

The nanodisk-spin system is a quasiferromagnet, which is an interpolating system between a single spin and a ferromagnet. It is easy to control a single spin by a tiny current but it does not hold the spin direction for a long time. On the other hand, a ferromagnet is very stable, but it is hard to control the spin direction by a tiny current. A nanodisk

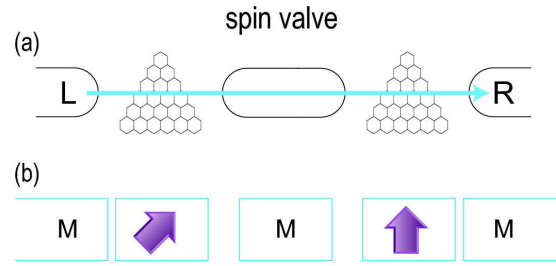


FIG. 6. The spin valve is made of two nanodisks with the same size, which are connected to leads. Applying an external magnetic field, we control the spin direction of the first nanodisk to be $|\theta\rangle$ and that of the second nanodisk to be $|\uparrow\rangle$. The incoming current is unpolarized, but the outgoing current is polarized and its magnitude can be controlled continuously. This acts as a spin valve.

quasiferromagnet has an intermediate nature: It can be controlled by a relatively tiny current and yet holds the spin direction for quite a long time⁵. Taking advantage of these properties we have already proposed elsewhere¹¹ some applications of graphene nanodisk-lead systems to spintronic devices. They are spin filter, spin memory, spin amplifier, spin valve, spin-field-effect transistor, spin diode and spin switch, among which here we make a concise review of spin filter, spin valve and spin switch. We newly propose nanodisk arrays and nanomechanical switch.

Spin filter: We consider a lead-nanodisk-lead system [see Fig.1(b)], where an electron makes a tunnelling from the left lead to the nanodisk and then to the right lead. This system is a reminiscence of a metal-ferromagnet-metal junction [see Fig.5]. If electrons in the lead has the same spin direction as the nanodisk spin, they can pass through the nanodisk freely. However, those with the opposite direction feel a large Coulomb barrier and are blocked (Pauli blockade [Fig.5(c)])¹¹. As a result, when we apply a spin-unpolarized current to the nanodisk, the outgoing current is spin polarized to the direction of the nanodisk spin. Consequently, this system acts as a spin filter.

Spin valve: A nanodisk can be used as a spin valve, inducing the giant magnetoresistance effect. We set up a system composed of two nanodisks sequentially connected with leads [see Fig.6]. We apply external magnetic field, and control the spin direction of the first nanodisk to be $|\theta\rangle = \cos \frac{\theta}{2} |\uparrow\rangle + \sin \frac{\theta}{2} |\downarrow\rangle$, and that of the second nanodisk to be $|0\rangle = |\uparrow\rangle$. We inject an unpolarized-spin current to the first nanodisk. The spin of the lead between the two nanodisks is polarized into the direction of $|\theta\rangle$. Subsequently the current is filtered to the up-spin one by the second nanodisk. The outgoing current from the second nanodisk is $I_{\uparrow}^{\text{out}} = I \cos \frac{\theta}{2}$. We can control the magnitude of the up-polarized current from 0 to I by rotating the external magnetic field. The system act as a spin valve.

Spin switch: We consider a chain of nanodisks and leads connected sequentially [see Fig.7]. Without external magnetic field, nanodisk spins are oriented randomly due to thermal fluctuations, and a current cannot go through the chain. However, when and only when a uniform magnetic field is applied

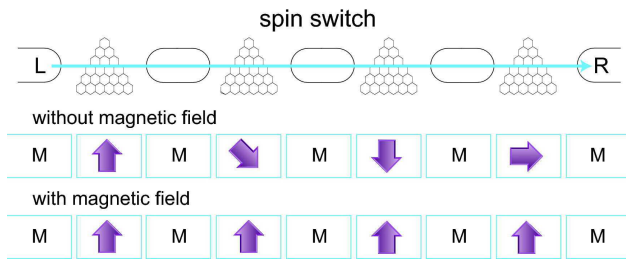


FIG. 7. A chain of nondisk and leads acts as a spin switch. Without external magnetic field, nanodisk spins are oriented randomly due to thermal fluctuations, and a current cannot go through the chain. However, as soon as a uniform magnetic field is applied to all nanodisks, the direction of all nanodisk spins become identical and a current can go through.

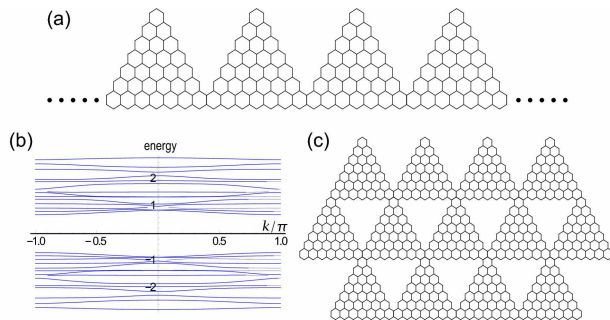


FIG. 8. (a) Illustration of one-dimensional nanodisk arrays. (b) Band structure of one-dimensional nanodisk arrays. (c) Illustration of two-dimensional nanodisk arrays.

to all nanodisks, the direction of all nanodisk spins become identical and a current can go through. Thus the system acts as a spin switch, showing a giant magnetoresistance effect. The advantage of this system is that a detailed control of magnetic field is not necessary in each nanodisk.

Nanodisk arrays: We investigate nanodisk arrays, which are materials where nanodisks are connected in one- or two-dimensions. These structures have already been manufactured by etching a graphene sheet by Ni nanoparticles⁶. We show an example of a trigonal-zigzag-nanodisk array sharing one zigzag edge as in Fig.8(a). We show the corresponding band structure in Fig.8(b). It is intriguing that there are N -fold degenerate perfect flat bands in the nanodisk with size N . This fact is confirmed by Leib's theorem. Each nanodisk has spin $N/2$ and makes ferromagnetic coupling between two nanodisks. In the same way we can make two-dimensional nanodisk arrays. It is to be emphasized that they show ferromagnetism, and not quasiferromagnetism, though they are made of nonmagnetic materials. The perfect flat band will be robust even when electron interactions are introduced.

Nanomechanical switch: We construct a nanomechanical switch contacting two graphene trigonal corners [see Fig.9(a)]. We assume the angle between two corners is θ . This angle is tuned by an external mechanical force. The carbon-skeleton structure is made of σ -bonds, and is very rigid except for this rotational degree of freedom.

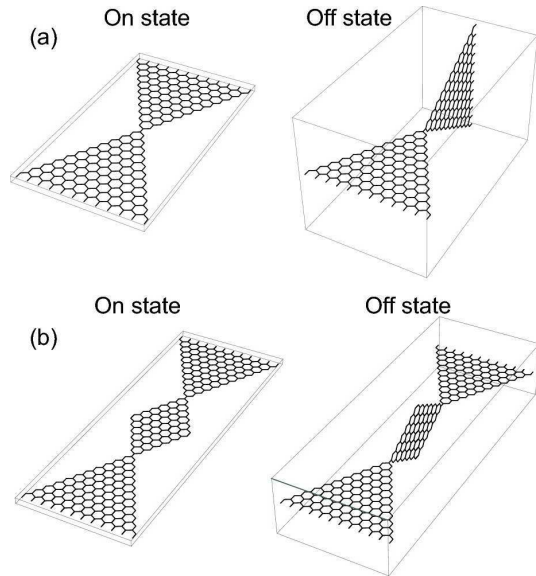


FIG. 9. (a) Illustration of a nanomechanical junction made of two triangular graphene corners. There are on and off states, switched by a rotation between two corners. (b) Illustration of a nanomechanical rotator made of two corners and a central rhombus rotating rather freely.

The conductance is determined by the overlap integral of π -electrons between two corners, which is given by

$$|\langle p_z \cos \theta + p_y \sin \theta | p_z \rangle| = \cos^2 \theta. \quad (18)$$

When the two planes are parallel ($\theta = 0$), the overlap takes the maximum value and π -electrons can go through the contact. This is the on state. When the two planes are orthogonal ($\theta = \pi/2$), the overlap takes the minimum value and π -electrons can not go through the contact. This is the off state. The angle is changed nanomechanically. The system acts as a nanomechanical switch. It could detect the angle very sensitively and be useful for detect nanomechanical oscillations.

By connecting two nanomechanical junctions, we can construct a nanomechanical rotator [Fig.9(b)], where two corners are suspended mechanically while the central rhombus rotates rather freely. This structure may be useful to detect molecular dynamics. When molecules contact the rotator, they are detected by rotating it and changing the resistance between the two corners.

Peierls instability: We connect two triangular corners with a zigzag nanoribbon [see Fig.10(a)]. This structure has already been manufactured experimentally⁶. Polyacetylene has the Peierls instability: Carbons with conjugate bonds are spontaneously deformed into alternating single and double bonds. We expect the Peierls instability to occur also in graphene nanoribbons [Fig.10(b)], because graphene nanoribbon is a natural extension of polyacetylene³. (We denote the width of a nanoribbon by W with $W = 0$ for polyacetylene and $W = 1$ for polyacene.) However, as we now show, the Peierls instability will not occur in nanoribbons with the width $W > 2$. On the contrary, it is possible to induce the Peierls transition manually by stretching a nanoribbon. Mak-

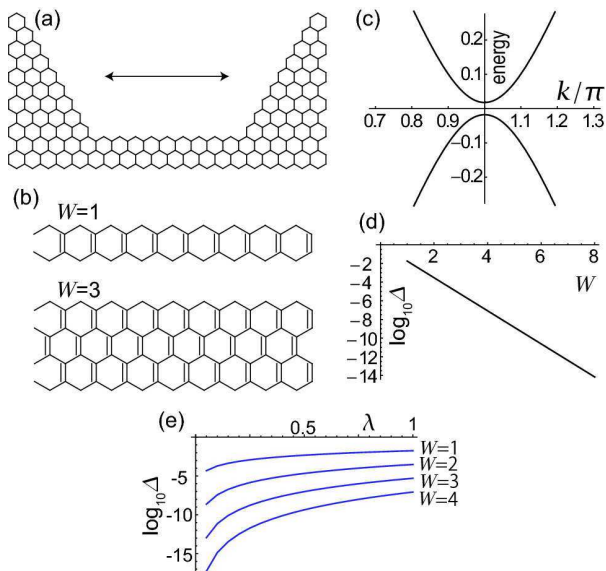


FIG. 10. (a) Illustration of a configuration where a single zigzag nanoribbon is connected by two triangular graphene corners. (b) Illustration of the Peierls instability of graphene nanoribbons with $W = 1$ and $W = 3$, where W represents the width. Single and double bonds alternatingly appears. (c) The band structure around $k = \pi$ of a polyacene with the Peierls instability. (d) The logarithm plot of the band gap Δ , $\log_{10} \Delta/t$, of nanoribbons with various W . (e) The logarithm plot of the band gap Δ , $\log_{10} \Delta/t$, of nanoribbons as a function of the applied force δ for various W .

ing an advantage of this property, we propose a nanomechanical switch sensor.

The model Hamiltonian is the Su-Schrieffer-Heeger-like model¹⁹,

$$H_0 = \sum_{\langle i,j \rangle} t_{ij} c_{i,\sigma}^\dagger c_{j,\sigma}. \quad (19)$$

In this model, when the Peierls instability occurs, the transfer integral takes two values corresponding to the single and double bonds, and otherwise it takes one value corresponding to the conjugate bond. We are able to calculate the gap analytically in the case of polyacene ($W = 1$), where the band structure around $k = \pi$ is given by

$$\varepsilon(k_x) = \pm \frac{1}{2} \left(-t_2 + \sqrt{4t_1^2 + 5t_2^2 + 8t_1 t_2 \cos k_x} \right). \quad (20)$$

The band gap is determined by substituting $k_x = \pi$ as

$$\Delta = 2\varepsilon(\pi) = \left(-t_2 + \sqrt{4t_1^2 + 5t_2^2 - 8t_1 t_2} \right) \sim 4\delta t_1 \delta t_2. \quad (21)$$

We show $\varepsilon(k_x)$ in Fig.10(c) by taking the values $t_1 = t - \delta t_1 = 0.94t$ for single bonds and $t_2 = t + \delta t_2 = 1.08t$ for double bonds. We have carried out a numerical estimation

of the band structure for $W \geq 2$. A tiny gap Δ opens at $k = \pi$. The logarithm plot of the band gap Δ as a function of the width W is shown in Fig.10(d). The gap decreases exponentially as a function of the width, $\propto 10^{-1.7W}$. The gap of the case $W = 1$ (polyacene) is 49meV, and that of the case $W = 2$ is 0.8meV.

We next compare the energy gain from this gap with the energy cost from the elastic energy of a lattice deformation. The ground-state energy difference between distorted and undistorted structures is very tiny in polyacene²⁰. On the other hand, the elastic energy cost is proportional to the width W , and hence the elastic energy cost becomes larger than the gap energy gain for wider nanoribbons. The Peierls instability will not occur spontaneously in nanoribbons with $W > 2$.

We have also estimated how the band gap Δ depends on the external force. The transfer integrals change proportionally to the external force. For simplicity we have set $t_1 = (1 - 0.06\lambda)t$ and $t_2 = (1 + 0.08\lambda)t$. It takes about 10GPa for deformation $0.01t$ for graphene, while it takes about 1GPa for deformation $0.01t$ for narrow graphene nanoribbons²¹. We show the logarithm plot of the λ dependence of the band gaps in Fig. 10(e).

We propose an application of the above system. By stretching a nanoribbon along the ribbon direction, horizontal bonds are stretched and vertical bonds are shrunk. The resultant structure is resemble to the deformed structure induced by the Peierls transition. We may call it a strain induced Peierls transition. When we stretch this structure, the band gap opens and the conductance at the zero energy becomes zero by the strain induced Peierls-transition. On the other hand, without the external mechanical force, nanoribbons with $W > 2$ is gapless and the system is conductive. We can switch the conductance from on to off by stretching the system. The system acts as a nanomechanical switch sensor detecting nanoscale displacement.

VII. CONCLUSIONS

A nanodisk can be used as a spin filter just as in a metal-ferromagnet-metal junction. A novel feature is that the direction of the spin can be controlled by external field or spin current. We have newly proposed nanodisk arrays and nanomechanical switch. These nanodisk-nanoribbon complex structure will open a new field of nanoelectronics, spintronics and nanoelectromechanics purely based on graphene.

Acknowledgements

I am very grateful to Y. Takada, H. Tsunetsugu, B.K. Nikolic and N. Nagaosa for fruitful discussions. This work was supported in part by Grants-in-Aid for Scientific Research from the Ministry of Education, Science, Sports and Culture No. 22740196 and 21244053.

References

-
- ¹ K. S. Novoselov, A. K. Geim, S. V. Morozov, D. Jiang, Y. Zhang, S. V. Dubonos, I. V. Grigorieva, and A. A. Firsov, *Science* **306**, 666 (2004). K. S. Novoselov, A. K. Geim, S. V. Morozov, D. Jiang, M. I. Katsnelson, I. V. Grigorieva, S. V. Dubonos and A. A. Firsov., *Nature* **438**, 197 (2005). Y. Zhang, Y.-W. Tan, Horst L. Stormer and Philip Kim, *Nature* **438**, 201 (2005).
 - ² M. Fujita, K. Wakabayashi, K. Nakada, and K. Kusakabe, *J. Phys. Soc. Jpn.* **65**, 1920 (1996).
 - ³ M. Ezawa, *Phys. Rev. B*, **73**, 045432 (2006).
 - ⁴ L. Brey, and H. A. Fertig, *Phys. Rev. B*, **73**, 235411 (2006).
 - ⁵ M. Ezawa, *Phys. Rev. B* **76**, 245415 (2007); M. Ezawa, *Physica E* **40**, 1421-1423 (2008); M. Ezawa, *New J. Phys.* **11**, 095005 (2009).
 - ⁶ L. C. Campos, V. R. Manfrinato, J. D. Sanchez-Yamagishi, J. Kong and P. Jarillo-Herrero, *Nano Lett.*, **9**, 2600 (2009).
 - ⁷ J. Fernández-Rossier, and J. J. Palacios, *Phys. Rev. Lett.* **99**, 177204 (2007).
 - ⁸ O. Hod, V. Barone, and G. E. Scuseria, *Phys. Rev. B* **77**, 035411 (2008).
 - ⁹ W. L. Wang, S. Meng and E. Kaxiras, *Nano Letters* **8**, 241 (2008).
 - ¹⁰ M. Ezawa, *Phys. Rev. B* **77**, 155411 (2008); *Phys. Rev. B* **79**, 241407(R) (2009).
 - ¹¹ M. Ezawa, *Eur. Phys. J. B* **67**, 543 (2009).
 - ¹² M. Ezawa, *Phys. Rev. B* **81**, 201402(R) (2010)
 - ¹³ W. L. Wang, Oleg V. Yazyev, S. Meng, and E. Kaxiras, *Phys. Rev. Lett.* **102**, 157201 (2009).
 - ¹⁴ J. Akola, H. P. Heiskanen, and M. Manninen, *Phys. Rev. B* **77**, 193410 (2008).
 - ¹⁵ O. V. Yazyev, *Rep. Prog. Phys* **73**, 5 (2010).
 - ¹⁶ A. D. Güçlü, P. Potasz, O. Voznyy, M. Korkusinski, and P. Hawrylak, *Phys. Rev. Lett.* **103**, 246805 (2009).
 - ¹⁷ P. Potasz, A. D. Güçlü and P. Hawrylak, *Phys. Rev. B* **81**, 033403 (2010).
 - ¹⁸ O. V. Yazyev and M. I. Katsnelson, *Phys. Rev. Lett.* **100**, 047209 (2008).
 - ¹⁹ W. P. Su, J. R. Schrieffer and A. J. Heeger, *Phys. Rev. B* **22**, 2099 (1980).
 - ²⁰ L. Salem and H. C. Longuet-Higgins, *Proc. R. Soc. London, Ser. A* **255**, 435 (1960).
 - ²¹ H. Zhao, K. Min, and N. R. Aluru, *Nano. Lett.* **9**, 3012 (2009).